Theory of the anomalous Doppler cyclotron-resonance-maser amplifier with tapered parameters

G. S. Nusinovich,[1] M. Korol,[2] and E. Jerby[2]
[1]*Institute for Plasma Research, University of Maryland, College Park, Maryland 20742*
[2]*Faculty of Engineering, Tel Aviv University, Ramat Aviv 69978, Israel*
(Received 5 June 1998)

The theory of a slow-wave cyclotron-resonance-maser (CRM) amplifier employing an initially linear electron beam is developed. In such a device, the electrons radiate electromagnetic waves under the anomalous Doppler effect. In order to maintain the cyclotron resonance between the radiating electrons and the amplifying electromagnetic wave, we consider a system with tapered waveguide parameters. The self-consistent set of equations results in one equation describing the efficiency of the anomalous Doppler CRM interaction as a function of the waveguide length. The efficiency limit approaches 100% in the ideal case. A practical scheme of the anomalous Doppler CRM amplifier is proposed as a stripline waveguide with a slight tapering of the strip width. This scheme is analyzed numerically, and it is shown that the efficiency of this device may exceed 30%. [S1063-651X(99)00302-5]

PACS number(s): 84.40.Ik, 52.75.Ms, 52.75.Va

I. INTRODUCTION

Cyclotron resonance masers (CRM's) are sources of coherent electromagnetic (EM) radiation based on the cyclotron resonance interaction between electrons gyrating in an external constant magnetic field and an EM wave (see, e.g., Refs. [1, 2]). A large number of various CRM's (including gyrodevices) are based on the operation when the normal Doppler effect takes place. In the cyclotron resonance condition,

$$\omega - k_z v_z \cong s\Omega, \tag{1}$$

this corresponds to the operating frequency ω larger than the Doppler term $k_z v_z$, so the resonance occurs at positive cyclotron harmonics ($s>0$). In Eq. (1) k_z is the axial wave number of the wave, and v_z and Ω, respectively, are the electron axial velocity and gyrofrequency. In CRM's based on the normal Doppler effect, the radiating electrons lose both orbital and axial components of their momentum (when $k_z \to 0$ the axial momentum remains unchanged). These devices have been studied in numerous papers (see, e.g., Refs. [1–5] and references therein). Much less attention has been paid to CRM's based on the anomalous Doppler effect.

In CRM's based on the anomalous Doppler effect (AD-CRM's) the Doppler term in Eq. (1) exceeds the frequency. This means that the phase velocity of the wave, $v_{\rm ph} = \omega/k_z$, is smaller than the electron axial velocity. Correspondingly, the resonant cyclotron harmonic number s should be negative. As is known [6], when oscillating electrons radiate EM waves under the anomalous Doppler effect, they lose their axial momentum and gain the orbital momentum.

The first approach to the theory of AD-CRM's was done in Ref. [7], where the interaction between ultrarelativistic gyrating electrons and a plane, transversely homogeneous, circularly polarized EM wave propagating in a medium with the refractive index $n = c/v_{\rm ph}$ was considered. In Ref. [7], as well as in Ref. [8], it was mentioned that the cyclotron radiation under the condition of the anomalous Doppler effect can be produced even by initially linear electron beams. (The same effect was also considered by Pierce when he studied the transverse motion of electrons in *O*-type traveling-wave tubes [9].) This is an important conclusion because the quality of linear electron beams formed by Pierce electron guns can be much better than that of the beams of gyrating electrons produced by magnetron injection guns. Also in Ref. [7], the range of parameters corresponding to the efficient operation of AD-CRM's was briefly discussed.

A systematic analysis of the same model of the AD-CRM was done in Ref. [10], where two configurations, a traveling-wave amplifier and a backward wave oscillator, were studied. It was found [10] that the maximum efficiency of the AD-CRM can be realized in the extreme case, when the external magnetic field is vanishingly small. Also, in the amplifier configuration, at large amplitudes of the input signal the electrons make only about one orbit in the interaction region before their departure from the cyclotron resonance due to the changes in electron energy. Such a regime of operation, certainly, cannot be realized at moderate voltages. Later, some experiments with AD-CRM's driven by relativistic electron beams were carried out [11–13], and some theoretical issues were also analyzed [14]. AD-CRM effects in periodic waveguides were discussed in Refs. [15, 16].

The issue of a practical realization of efficient AD-CRM's operating at reasonably low voltages, where electrons should make many orbits and efficiently interact with an EM wave of a moderate amplitude, has not yet been addressed. Since such a regime cannot be realized in AD-CRM's with constant parameters of the interaction region (which were studied earlier), we suggest to taper these parameters. In the present paper we consider an AD-CRM with a variable axial wave number of the wave, and show that such a device can efficiently operate at moderate voltages. The idea to taper $\mathbf{k}_z(z)$ to ensure the cyclotron resonance between the wave and decelerating electrons, certainly, is similar to the ideas of tapering the parameters of a slow-wave structure (SWS) used in isochronous traveling wave tubes [17,18] (see also Ref. [9], p. 167), tapering the wiggler parameters in free electron

lasers (FEL's) [19,20], and profiling the external magnetic field in relativistic gyrotrons [21] and traveling-wave CRM's [22].

In periodic slow-wave structures (the helix-type SWS, the coupled-cavity SWS, and waveguides with periodically corrugated walls) the tapering can be realized by a slow variation of the period. Another class of attractive slow-wave structures which can be tapered for our goals are stripline waveguides which were successfully used in FEL [23] and CRM [24] experiments. The stripline waveguides used in these experiments had a uniform cross section. The stripline waveguide has various advantages compared to conventional dielectrically loaded and periodic waveguides. Operation at the quasi-TEM mode provides a linear dispersion and, thus, the interaction may occur in a wide bandwidth of frequencies. Also, this mode eliminates parasitic Cherenkov interactions. From the technical point of view, the metallic strips protect the dielectric material from electron bombardment and charging. In this paper we suggest to taper the width of the strip in order to maintain the cyclotron resonance (1) along the interaction region. Analytical and numerical analysis may form a basis for further experimental design of the AD-CRM amplifier in the tapered stripline waveguide.

Our paper is organized as follows. In Sec. II we present a general formalism describing the AD-CRM with an arbitrary slow-wave structure and a tapered axial wave number k_z. Section III is devoted to the analysis of a practical scheme of the AD-CRM device employing the tapered stripline waveguide. Section IV demonstrates a numerical example, and Sec. V concludes our work.

II. GENERAL FORMALISM

Our consideration is based on the assumption that the tapering of the slow-wave circuit provides the exact cyclotron resonance between decelerating electrons and an EM wave. (A practical realization of this tapering is discussed in Sec. III.) The corresponding dependence of the optimal normalized axial wave number $h=k_z c/\omega$ on the electron energy and velocity, as follows from Eq. (1) for $s=-1$, can be determined as

$$h_{\mathrm{opt}}=\frac{1}{\beta_z}\left(1+\mu\,\frac{\gamma_0}{\gamma}\right). \tag{2}$$

Here β_z is the axial electron velocity normalized to the speed of light, μ is the ratio of the electron cyclotron frequency at injection to the operating frequency, and γ is the electron energy normalized to the rest energy. At the entrance to the interaction region,

$$h_{\mathrm{opt}}=h_0=\frac{1}{\beta_{z0}}\,(1+\mu). \tag{3}$$

Introducing normalized electron momentum $p'=p/m_0 c\,\gamma_0$ and the energy change function $w=(\gamma_0-\gamma)/\gamma_0$, and combining Eqs. (2) and (3), one can obtain the following equation for h_{opt}:

$$h_{\mathrm{opt}}=(h_0\beta_{z0}-w)/p'_z. \tag{4}$$

Below we will restrict our consideration by the analysis of interaction with TEM and TE waves. For these waves, as known (see, e.g., Refs. [7, 10, 5, 25, 26]), the changes in the electron energy and axial momentum are related as

$$h\,\frac{dw}{dz}+\frac{dp'_z}{dz}=0. \tag{5}$$

When the axial wave number is constant, from Eq. (5) one obtains the autoresonance integral [27–29]

$$hw+p'_z=\beta_{z0}. \tag{6}$$

When the optimally tapered h obeys Eq. (4), from Eq. (5) one can obtain the following relation between electron energy and axial momentum:

$$p'^2_z=\beta^2_{z0}-2h_0\beta_{z0}w+w^2. \tag{7}$$

Correspondingly, from the general equation $\gamma^2=1+\gamma_0^2(p'^2_\perp+p'^2_z)$ one can derive for the orbital momentum of an electron with initial zero orbital velocity the following equation:

$$p'^2_\perp=2(h_0\beta_{z0}-1)w=2\mu w. \tag{8}$$

Equations (7) and (8) establish the relations between the changes in the electron energy and components of electron momentum. For initially gyrating electrons the corresponding equations are given elsewhere [22].

Since the electrons radiating EM waves under the condition of the anomalous Doppler effect lose their axial momentum and gain the orbital momentum [6], the maximum energy which can be withdrawn from a radiating electron corresponds to $p_z=0$ in the final stage. As follows from Eq. (7), the corresponding maximum value of the electron efficiency,

$$\eta=\frac{1}{1-\gamma_0^{-1}}\,w, \tag{9}$$

is equal to

$$\eta_{\max}=\left(\frac{\gamma_0+1}{\gamma_0-1}\right)^{1/2}(h_0-\sqrt{h_0^2-1}). \tag{10}$$

Note that, in accordance with Eq. (4), to realize $p_z\to 0$ one should operate at infinitely large h's. Since in experiments h is always limited by a certain finite value $h_{\max}$, the corresponding maximum efficiency is determined by

$$\eta_{\max}=\left(\frac{\gamma_0+1}{\gamma_0-1}\right)^{1/2}[h_0-\sqrt{(h_0^2-1)/(1-h_{\max}^{-2})}]. \tag{11}$$

Also note that using the cyclotron resonance condition given by Eq. (3), Eq. (10) can be rewritten as

$$\eta_{\max}=\frac{1}{1-\gamma_0^{-1}}\,[1+\mu-\sqrt{(1+\mu)^2-(1-\gamma_0^{-2})}]. \tag{12}$$

In a similar way one can also rewrite Eq. (11).

Recall that in the case of the tapered slow-wave structure the electrons stay in the region of the anomalous Doppler

effect during all the process of their deceleration (in contrast to the case of a constant h [10]). Correspondingly, when electrons lose all the axial momentum their orbital momentum is equal to $p'_\perp=\sqrt{2\mu w_{\max}}$. This agrees with Eq. (12), from which it follows that $\eta_{\max}\to 1$ when $\mu\to 0$, i.e., in optimal regimes the magnetic field should be small.

After these preliminary remarks we can consider the equations describing the evolution of the normalized electron energy change w, the normalized orbital momentum $p'_\perp$, the slowly variable phase $\theta=k_z z-\omega t-\vartheta$ (ϑ is the electron gyrophase), and the normalized wave amplitude along the normalized axial coordinate $z'=\omega z/c$ (below, the primes in $p'_{\perp,z}$ and z' will be omitted). Corresponding expressions for the components of the Lorentz force with which the wave acts on gyrating electrons were derived elsewhere [25,26,30]. We will represent the electric field of the wave as $\vec{E}=\mathrm{Re}\{A(z)\vec{E}_c(\vec{r})\exp[i(\omega t-k_z z)]\}$. Here the vector function $\vec{E}_c(\vec{r})$ describes the transverse structure of the wave electric field, and can be represented as $\vec{E}_c=ik\nabla\Psi\times\hat{z}$ where the membrane function $\Psi(\vec{r})$ is the solution of the Helmholtz equation

$$\Delta_\perp\Psi+k_\perp^2\Psi=0, \tag{13}$$

with the corresponding boundary condition. In Eq. (13), $k_\perp=\omega_c/c$ is the transverse wave number and ω_c is the cutoff frequency. The components of the Lorentz force, as can be found elsewhere [25,26,30], are proportional to the wave amplitude A, to the coefficient

$$L_s=\left[\frac{1}{k_\perp}\left(\frac{\partial}{\partial X}+i\,\frac{s}{|s|}\,\frac{\partial}{\partial Y}\right)\right]^{|s|}\Psi(X,Y), \tag{14}$$

which describes the transverse structure of the Lorentz force acting on an electron with transverse coordinates of the guiding center X and Y, and to the Bessel functions $J_s(\xi)$ and their derivatives $J'_s(\xi)$ (here $\xi=k_\perp r_L$, and $r_L=v_\perp/\Omega$ is the Larmor radius of electron). This representation of the Lorentz force components stems from the multipole nature of the EM field rotating synchronously with gyrating electrons. In our case $s=-1$, so

$$L_{-1}=\frac{1}{k_\perp}\left(\frac{\partial}{\partial X}-i\,\frac{\partial}{\partial Y}\right)\Psi(X,Y). \tag{15}$$

We will also assume that the normalized gyroradius ξ is small enough ($\xi^2\ll 1$), and hence, $J_{-1}(\xi)=-J_1(\xi)\cong-\xi/2$.

Under these assumptions a self-consistent set of gyro-averaged equations describing a properly tapered traveling-wave AD-CRM with an initially linear electron beam can be written as

$$\frac{dp_\perp}{dz}=\frac{h\beta_z-1}{\beta_z}\,\mathrm{Re}\left\{\frac{A'L_{-1}}{2\kappa}\,e^{-i\theta}\right\}, \tag{16a}$$

$$p_\perp\,\frac{d\theta}{dz}=-\frac{h\beta_z-1}{\beta_z}\,\mathrm{Re}\left\{i\,\frac{A'L_{-1}}{2\kappa}\,e^{-i\theta}\right\}, \tag{16b}$$

$$\frac{dw}{dz}=\frac{p_\perp}{p_z}\,\mathrm{Re}\left\{\frac{A'L_{-1}}{2\kappa}\,e^{-i\theta}\right\}, \tag{16c}$$

$$\frac{dA'}{dz}=\frac{eI_b}{m_0c^3\gamma_0}\,\frac{c^3}{\omega^2N}\left\langle\frac{L^*_{-1}}{2\kappa}\,\frac{p_\perp}{p_z}\,e^{i\theta}\right\rangle, \tag{16d}$$

where $A'=eA/m_0c\omega\gamma_0$ and $\kappa=k_\perp c/\omega$ are the normalized wave amplitude and the normalized transverse wave number, respectively. (The derivation of similar equations for various versions of CRM amplifiers is given elsewhere [5,22,30,31].) In Eq. (16d), I_b is the beam current, angular brackets mean averaging over the beam cross section, and

$$N=\frac{c}{2\pi}\,\frac{(\omega/c)^2h}{k_\perp^4}\int_{S_\perp}|\nabla_\perp\Psi|^2\,dS_\perp \tag{17}$$

is the norm of the wave. Now, let us denote $A'L_{-1}/2\kappa$ by $Fe^{i\alpha}$, where F and α are, respectively, the absolute value and phase of this combination, and introduce

$$I_0=\frac{eI_b}{m_0c^3\gamma_0}\,\frac{|L_{-1}|^2}{4\kappa^2}\,\frac{c^3}{\omega^2N}. \tag{18}$$

Here and below we will consider a beam of electrons for which the transverse inhomogeneity of the wave Lorentz force is not important. Correspondingly, the transverse drift of electron guiding centers can be ignored (see, e.g., Ref. [30]), and L_{-1} can be considered as a constant value. This allows us to rewrite Eqs. (16a)–(16d) in the following forms:

$$\frac{dp_\perp}{dz}=\frac{h\beta_z-1}{\beta_z}\,F\,\cos\,\overline{\theta}, \tag{19a}$$

$$\frac{dw}{dz}=\frac{p_\perp}{p_z}\,F\,\cos\,\overline{\theta}, \tag{19b}$$

$$\frac{dF}{dz}=I_0\,\frac{p_\perp}{p_z}\,\cos\,\overline{\theta}, \tag{19c}$$

$$\frac{d\overline{\theta}}{dz}=-\left(\frac{I_0}{F}+\frac{F}{2w}\right)\frac{p_\perp}{p_z}\,\sin\,\overline{\theta}. \tag{19d}$$

Here $\overline{\theta}=\theta-\alpha$, so Eq. (19d) is obtained by superposition of Eq. (16b) and the imaginary part of Eq. (16d).

Equations (19b) and (19c), properly combined, yield the energy conservation law for the system ''electron beam plus EM wave''

$$F^2-F_0^2=2\int_0^z I_0\,\frac{dw}{dz'}\,dz', \tag{20}$$

which in the case of a constant I_0 reduces to the standard (see, e.g., Refs. [10, 25]) form $F^2-F_0^2=2I_0w$. In Eq. (20) and below, F_0 is the wave amplitude at the entrance. Note that the gain of the device, $G=20\log_{10}(F/F_0)$, can be large only when the normalized current I_0 is large enough.

Also note that when h and $p_\perp$ obey, respectively, Eqs. (2) and (8), one can rewrite Eq. (19d) using Eqs. (19a) and (19c) as

$$\frac{d\overline{\theta}}{dz} = -\frac{\sin\overline{\theta}}{\cos\overline{\theta}}\frac{1}{p_\perp F}\frac{d(p_\perp F)}{dz}.$$

From here one can readily derive the equation

$$\frac{d}{dz}(p_\perp F \sin\overline{\theta}) = 0,$$

which gives the integral of motion

$$p_\perp F \sin\overline{\theta} = \text{const.} \tag{21}$$

Since at the entrance $p_\perp = 0$ to fulfill Eq. (21) for nonzero $p_\perp$'s in the process of interaction, it is necessary to have $\overline{\theta} = 0$. This conclusion makes the device under study quite different from previously analyzed CRM's with tapered parameters operating in the region of the normal Doppler effect where the tapering should provide the condition of synchronism for a so-called ''synchronous'' electron around which an electron bunch is formed. In those devices with initially gyrating electrons the stationary phase of the synchronous electron need not be equal to zero. Therefore, for any initial amplitude of the wave F_0 the initial phase $\overline{\theta}_0$ can be chosen so that $F_0 \sin\overline{\theta}_0$ will be the same, as pointed out in Ref. [31]. Correspondingly, the changes in the electron energy and thus the tapering given by Eq. (2) can be the same for any F_0. On the contrary, the operation of the AD-CRM with an initially linear electron beam, as follows from our conclusion about $\overline{\theta} = 0$, seems to be sensitive to the input power.

Now we can come back to the set of Eqs. (19a)–(19d), and note that assuming $\overline{\theta} = 0$, and using Eqs. (7) and (8) for p_z and $p_\perp$, respectively, and the balance equation (20) for F, we can reduce this set of equations to one equation for the normalized electron energy change. To do this we should, in particular, specify the tapering of the normalized current parameter I_0 in Eq. (20). Below we will assume that the device operates at frequencies not so far from the cutoff frequency ω_c where $h^2 \ll 1$, and hence $\kappa^2 \approx 1$. This means that the tapering of a slow-wave structure may cause significant changes in the normalized current parameter I_0 only due to the tapering of h [see Eqs. (17) and (18)], while the changes in $k_\perp^2$ are negligibly small. Then, as follows from Eqs. (17), (18), (4), and (7), the normalized current parameter can be represented as

$$I_0 = I_{00}\frac{h_0}{h_0\beta_{z0} - w}\sqrt{\beta_{z0}^2 - 2h_0\beta_{z0}w + w^2}, \tag{22}$$

where I_{00} is the value of I_0 at the entrance. Since Eq. (22) determines the dependence of I_0 on w it is reasonable to rewrite the right-hand side of Eq. (20) as

$$2\int_0^w I_0(w')dw' = 2I_{00}h_0\int_0^w \frac{\sqrt{\beta_{z0}^2 - 2h_0\beta_{z0}w' + w'^2}}{h_0\beta_{z0} - w'}dw'. \tag{23}$$

This integral, as follows from Ref. [32], is equal to

$$f(w) + (h_0^2-1)^{1/2}\beta_{z0}\arcsin\left[\frac{(h_0^2-1)^{1/2}f(w)}{h_0(h_0\beta_{z0}-w)}\right], \tag{24}$$

where the function $f(w) = \beta_{z0} - \sqrt{\beta_{z0}^2 - 2h_0\beta_{z0}w + w^2}$, as follows from Eq. (7), describes the changes in the normalized axial momentum. In accordance with Eqs. (23) and (24), the wave amplitude can be determined from Eq. (20) as

$$F = F_0\left[1 + I\left\{f + (h_0^2-1)^{1/2}\beta_{z0}\arcsin\left[\frac{(h_0^2-1)^{1/2}f}{h_0(h_0\beta_{z0}-w)}\right]\right\}\right]^{1/2}, \tag{25}$$

where $I = 2h_0I_{00}/F_0^2$. Now we can come back to Eq. (19b), introduce the normalized axial coordinate $\zeta = F_0 z$ and, using Eqs. (25), (7) and (8), rewrite it as

$$\frac{dw}{d\zeta} = \left\{\frac{2(h_0\beta_{z0}-1)w}{\beta_{z0}^2 - 2h_0\beta_{z0}w + w^2}\left[1 + I\left\{f + (h_0^2-1)^{1/2} \times \beta_{z0}\arcsin\left[\frac{(h_0^2-1)^{1/2}f}{h_0(h_0\beta_{z0}-w)}\right]\right\}\right]\right\}^{1/2}. \tag{26}$$

By solving only this equation with three parameters h_0, β_{z0}, and I, one can study the axial evolution of the electron energy and, correspondingly, calculate the efficiency given by Eq. (9). [Recall that γ_0 in Eq. (9) and β_{z0} in Eq. (26) are related as $\gamma_0 = 1/\sqrt{1-\beta_{z0}^2}$]. By inverting Eq. (26) one can also find the length ζ_c required for complete deceleration of electrons $\zeta_c = \int_0^{1-\gamma_0^{-1}}[1/F(w)]dw$. Here $F(w)$ denotes the right-hand side of Eq. (26).

Results of numerical calculation of Eq. (26) are shown in Figs. 1, 2, and 3. Figures 1(a) and 1(b), respectively, show the dependence of the efficiency η [defined by Eq. (9)] and the corresponding tapering of the normalized axial wave number h [derived from Eqs. (4) and (7)] on the normalized axial coordinate ζ for different initial values of $\beta_{z0}h_0$. In these calculations, the accelerating voltage V_b and initial current parameter I are equal to 40 kV and 100, respectively. Figures 2(a) and 2(b) show, respectively, the dependence of the efficiency and the axial wavenumber on the axial distance for different values of the current parameter I, whereas the accelerating voltage and the parameter $\beta_{z0}h_0$ are constant and equal to 40 kV and 1.1, respectively. It should be noted that the cases of different values of the current parameter differ only by the interaction length ζ, whereas the efficiency and wavenumber remain unchanged. Figures 3(a) and 3(b) show the efficiency and axial wave number, respectively, as functions of the coordinate ζ for different voltages V_b and constant $I(100)$ and $\beta_{z0}h_0(1.1)$.

Before closing this section let us note that Eq. (26) does not contain the initial amplitude of the wave, F_0; however, the coordinate ζ is normalized to F_0. So the solution obtained for a fixed ζ will correspond, in the case of different F_0's, to different axial positions.

III. ANOMALOUS DOPPLER CRM INTERACTION IN A TAPERED STRIPLINE WAVEGUIDE

A practical scheme for the anomalous Doppler CRM amplifier is proposed in this section. This scheme employs a

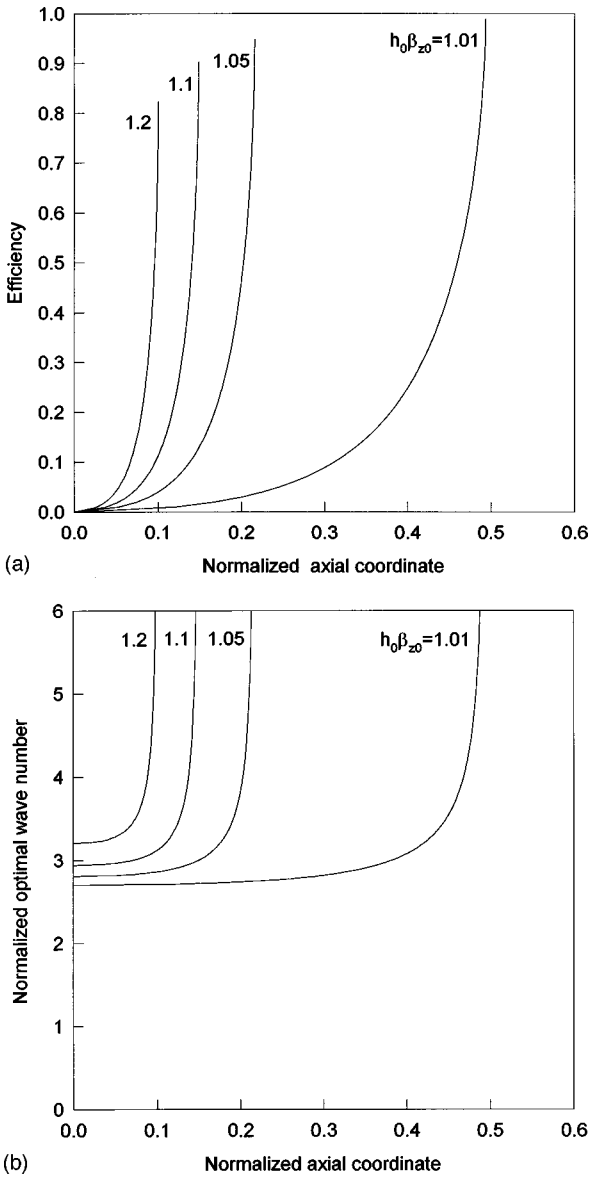

FIG. 1. The dependence of the maximal efficiency η (a) and optimal wave number h (b) on the normalized axial coordinate ζ for different initial values of $h_0\beta_{z0}$. The accelerating voltage V_b and normalized initial current parameter I are 40 kV and 100, respectively.

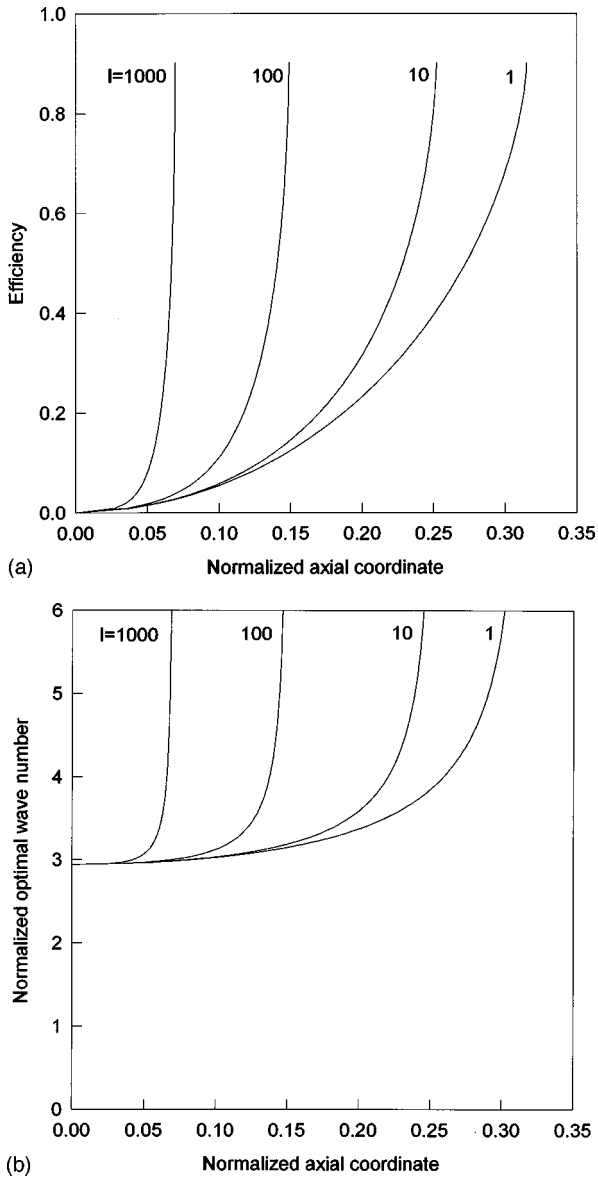

FIG. 2. The dependence of the maximal efficiency η (a) and optimal wave number h (b) on the normalized axial coordinate ζ for different initial values of the normalized initial current parameter I. The accelerating voltage V_b and parameter $h_0\beta_{z0}$ are 40 kV and 1.1, respectively.

stripline waveguide with a slight tapering of the strip width along the interaction region. The proposed device and the waveguide cross-section are shown schematically in Figs. 4(a) and 4(b), respectively.

Striplines and microstrips are commonly used as transmission lines in modern microwave integrated circuits [33]. The fundamental mode of the stripline is the hybrid EM mode, and various analytical and numerical methods have been developed in order to find the exact wave solution (including axial components) in such structures [34–36]. Nevertheless, at low frequencies (when the transverse sizes of the stripline are smaller than the wavelength) the wave propagating along the stripline can be approximated by a quasi-TEM mode with a linear dispersion [33,37]. Its transverse wave number $k_\perp$ is negligible. Consequently, Eqs. (16a)–(16d), (17), and (18) must be rewritten for the quasi-TEM mode in order to exclude the transverse wave number from the expressions. Also the normalized amplitude F must be redefined. The general expressions describing the anomalous Doppler CRM interaction ($s=-1$) could be written in the forms

$$\frac{dp_\perp}{dz} = -\frac{1}{\beta_z}\,\mathrm{Re}\{A'[E_{-1\theta}+\beta_z H_{-1r}]e^{-i\theta}\}, \tag{27a}$$

$$p_\perp \frac{d\theta}{dz} = -\frac{1}{\beta_z}\,\mathrm{Re}\{A'[E_{-1r}+\beta_\theta H_{-1z}-\beta_z H_{-1\theta}]e^{-i\theta}\}, \tag{27b}$$

$$\frac{dw}{dz} = \frac{p_\perp}{p_z}\,\mathrm{Re}\{A' E_{-1\theta} e^{-i\theta}\}, \tag{27c}$$

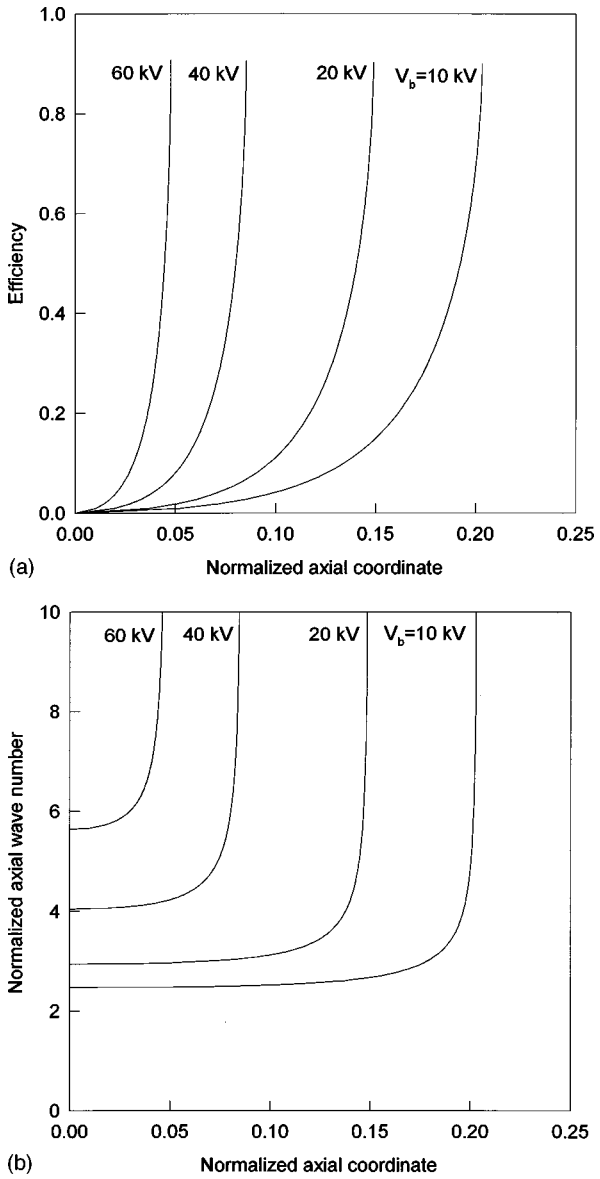

FIG. 3. The dependence of the maximal efficiency η (a) and optimal wave number h (b) on the normalized axial coordinate ζ for different initial values of the accelerating voltage V_b. The initial values of the normalized current parameter I and parameter $h_0\beta_{z0}$ are 100 and 1.1, respectively.

$$\frac{dA'}{dz}=\frac{eI_b}{m_0c^3\gamma_0}\frac{c^3}{\omega^2 N}\left\langle E^*_{-1\theta}\frac{p_\perp}{p_z}e^{i\theta}\right\rangle. \tag{27d}$$

In Eqs. (27a)–(27d), $E_{-1r}, E_{-1\theta}, H_{-1r}, H_{-1\theta}$, and H_{-1z} are polar projections of coefficients $\vec{E}_{-1}$ and $\vec{H}_{-1}$ in the coordinate frame associated with the guiding center X, Y of electron gyromotion. These vectors $\vec{E}_{-1}$ and $\vec{H}_{-1}$ are related to the functions describing the transverse distribution of electric, $\vec{E}_c$, and magnetic, $\vec{H}_c$, fields [see the representation of electric field given above, before Eq. (13)], as

$$\vec{E}_{-1}=\frac{1}{2\pi}\int_0^{2\pi}\vec{E}_c e^{-i\vartheta}d\vartheta \tag{28a}$$

and

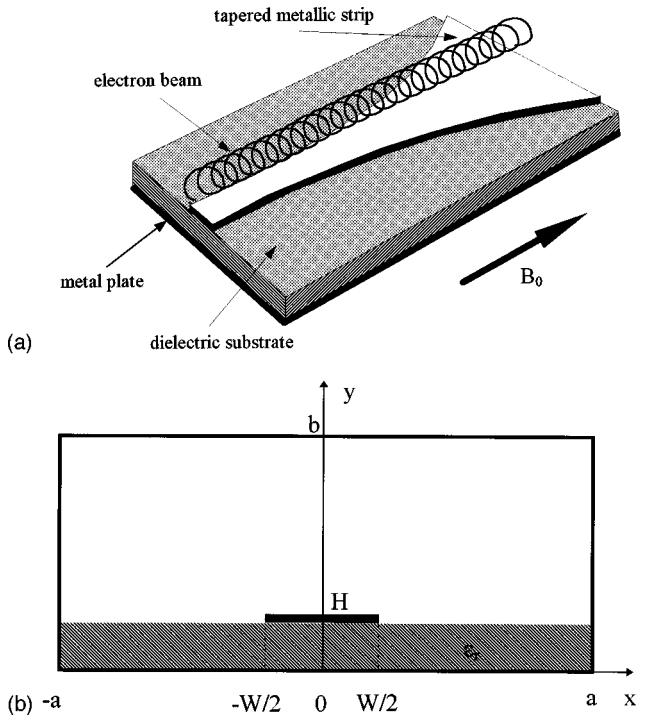

FIG. 4. (a) Schematic of an anomalous Doppler CRM amplifier with a tapered stripline waveguide (the side and upper waveguide walls are omitted in this drawing). (b) Schematic of the stripline waveguide cross section.

$$\vec{H}_{-1}=\frac{1}{2\pi}\int_0^{2\pi}\vec{H}_c e^{-i\vartheta}d\vartheta. \tag{28b}$$

Here ϑ is the electron gyrophase introduced in Sec. II, which can also be treated as the azimuthal coordinate in the reference frame associated with the electron guiding center. The corresponding expression for the norm of the wave, N, is given by

$$N=\frac{c}{4\pi}\int_{S_\perp}\{[\vec{E}_c\times\vec{H}^*_c]-[\vec{H}_c\times\vec{E}^*_c]\}\cdot\hat{z}\,dS_\perp. \tag{29}$$

For pure TE or TEM modes,

$$E_{-1\theta}+\beta_z H_{-1r}=(1-h\beta_z)E_{-1\theta} \tag{30a}$$

and

$$E_{-1\theta}+\beta_z H_{-1r}=i(E_{-1r}+\beta_\perp H_{-1z}-\beta_z H_{-1\theta}), \tag{30b}$$

and from the equation set (27a)–(27d) we arrive at Eqs. (16a)–(16d). (Note that for the TEM mode, $H_{-1z}=0$). The quasi-TEM mode is not a rigorous mode, but a practical approximation of it. Hence Eq. (30a) is not satisfied exactly for the quasi-TEM mode, although Eq. (30b) still holds. This is a consequence of the transverse inhomogeneity of the waveguide partially filled by the dielectric material. Nevertheless, at low frequencies the quasi-TEM mode approximation is close to the real EM field of the stripline, and we can assume that Eq. (30a) is valid. Hence taking $E_{-1\theta}$ as the source function, we define the current parameter as

$$I_0=\frac{eI_b}{m_0c^3\gamma_0}\,|E_{-1\theta}|^2\,\frac{c^3}{\omega^2 N}, \tag{31}$$

and the amplitude F and phase α by $Fe^{i\alpha}=A'E_{-1\theta}$. Then we arrive at the same set of equations (19a)–(19d) as for the exact mode.

To specify parameters in Eq. (26) for numerical calculations, one needs to derive analytical expressions for $\vec{E}_c$, $\vec{H}_c$, and $E_{-1\theta}$ (they are included in the expression for the current parameter I). This can be done by using the wave analysis of a cold stripline waveguide. In this analysis we assume that the tapered width of the strip W is slowly varying along the axis. Hence the local solution for the axially uniform strip provides a reasonable approximation for the tapered stripline waveguide.

A general method for the stripline analysis is presented in Ref. [33]. The axial wavenumber k_z of the fundamental quasi-TEM wave is given by

$$k_z=\sqrt{\varepsilon_{\rm eff}}\,\frac{\omega}{c}, \tag{32}$$

where the effective permittivity $\varepsilon_{\rm eff}$ depends on the transverse geometry of the stripline waveguide and on the relative permittivity ε_r of the dielectric substrate. It is defined by

$$\varepsilon_{\rm eff}=\frac{Q}{Q_0}, \tag{33}$$

where Q and Q_0 are the total linear charges on the strip of the stripline waveguide and corresponding air-filled stripline waveguide (without dielectric material inside), respectively. The values of Q and Q_0 are obtained using a Fourier series expansion method as follows. The charge density on the strip, $\rho(\mathbf{x})$, can be expressed as an infinite sum of transverse harmonics,

$$\rho(x)=\sum_{n=1,3,\ldots}\rho_n\cos(\omega_n x), \tag{34a}$$

where its harmonics coefficients ρ_n are given by

$$\rho_n=\frac{1}{a}\int_{-W/2}^{W/2}\rho(x)\cos(\omega_n x)\,dx. \tag{34b}$$

In Eqs. (34), a is the half of the waveguide width and $\omega_n=\pi n/2a$. Assuming that the voltage on the strip and waveguide walls is $V\neq 0$ and zero, respectively, the charge density $\rho(x)$ is obtained from the integral equation

$$\frac{4\pi}{aV}\sum_{n=1,3,\ldots}\frac{\sinh(\omega_n H)\sinh(\omega_n(b-H))}{\omega_n T_n}\cos(\omega_n x)\times\int_{-W/2}^{W/2}\rho(x')\cos(\omega_n x')\,dx'=1, \tag{35a}$$

where the harmonic coefficients T_n are defined as

$$T_n=\sinh(\omega_n H)\cosh(\omega_n(b-H))+\varepsilon_r\cosh(\omega_n H)\sinh(\omega_n(b-H)), \tag{35b}$$

and b and H are heights of the waveguide and dielectric medium, respectively, as shown in Fig. 4(b). The integral equation (35a) holds for each x in the interval $[-W/2;W/2]$ and can be solved by various numerical methods. Finally, the total linear charge Q is obtained by integrating the charge density $\rho(x)$ given by Eq. (34a) over the strip width as follows:

$$Q=2\sum_{n=1,3,\ldots}\frac{\rho_n}{\omega_n}\sin\left(\omega_n\frac{W}{2}\right). \tag{36}$$

The total charge on the strip in the air-filled waveguide, Q_0, is obtained by a similar procedure as for Q with $\varepsilon_r=1$ everywhere inside the waveguide. Note that in addition to the straightforward calculation of the effective permittivity described above, several approximate formulas have been derived [33,37].

The electric and magnetic components of the quasi-TEM mode are determined by the electrostatic potential Φ, and the axial component of the vector potential, A_z, respectively. These potentials obey Laplace equations

$$\nabla_\perp^2\Phi=0 \tag{37a}$$

and

$$\nabla_\perp^2 A_z=0. \tag{37b}$$

The potential functions are zero on the waveguide walls and constant on the metal strip surface. The normal derivative of the electromagnetic potential A_z is continuous on the interface between the vacuum and dielectric regions, and has a step change on the strip surface, whereas the normal derivative of the electrostatic potential Φ is not continuous on both the strip and dielectric surface. Note that boundary conditions for the electrostatic potential Φ have been used in the derivation of Eq. (35a). Using Eqs. (34) and (35), the potential functions Φ and A_z can be expressed as

$$\Phi(x,y)=4\pi\sum_{n=1,3,\ldots}\frac{\rho_n\phi_n(x,y)}{\omega_n T_n} \tag{38a}$$

and

$$A_z(x,y)=\frac{4\pi}{\sqrt{\varepsilon_{\rm eff}}}\sum_{n=1,3,\ldots}\frac{\rho_n\phi_n(x,y)}{\omega_n\sinh(\omega_n b)}, \tag{38b}$$

respectively, where the harmonic profile functions ϕ_n are defined as follows:

$$\phi_n(x,y)=\cos(\omega_n x)\times\begin{cases}\sinh(\omega_n(b-H))\sinh(\omega_n y), & y\leqslant H\\ \sinh(\omega_n H)\sinh(\omega_n(b-y)), & H\leqslant y\leqslant b.\end{cases} \tag{39}$$

The transverse electric and magnetic fields are obtained from Eqs. (38a) and (38b) as follows:

$$E_{xc}(x,y)=\frac{4\pi}{|\vec{E}|}\sum_{n=1,3,\ldots}\frac{\rho_n\varphi_n(x,y)}{T_n}, \tag{40a}$$

$$E_{yc}(x,y)=\frac{4\pi}{|\vec{E}|}\sum_{n=1,3,\ldots}\frac{\rho_n\psi_n(x,y)}{T_n}, \tag{40b}$$

$$H_{xc}(x,y)=-\frac{4\pi}{|\vec{H}|\sqrt{\varepsilon_{\mathrm{eff}}}}\sum_{n=1,3,\ldots}\frac{\rho_n\psi_n(x,y)}{\sinh(\omega_n b)}, \tag{41a}$$

$$H_{yc}(x,y)=\frac{4\pi}{|\vec{H}|\sqrt{\varepsilon_{\mathrm{eff}}}}\sum_{n=1,3,\ldots}\frac{\rho_n\varphi_n(x,y)}{\sinh(\omega_n b)}, \tag{41b}$$

where the harmonic transverse profiles φ_n and ψ_n are defined as

$$\varphi_n(x,y)=\sin(\omega_n x)\times\begin{cases}\sinh(\omega_n(b-H))\sinh(\omega_n y), & y\leqslant H,\\ \sinh(\omega_n H)\sinh(\omega_n(b-y)), & H\leqslant y\leqslant b\end{cases} \tag{42a}$$

and

$$\psi_n(x,y)=\cos(\omega_n x)\times\begin{cases}-\sinh(\omega_n(b-H))\cosh(\omega_n y), & y\leqslant H,\\ \sinh(\omega_n H)\cosh(\omega_n(b-y)), & H\leqslant y\leqslant b,\end{cases} \tag{42b}$$

respectively, and the amplitudes $|\vec{E}|$ and $|\vec{H}|$ correspond to the maximal values of these fields inside the waveguide cross section. The term $E_{-1\theta}$ can be derived from Eqs. (40a) and (40b) as follows:

$$E_{-1\theta}=\frac{2\pi}{|\vec{E}|}\sum_{n=1,3,\ldots}\frac{\rho_n}{T_n}\sinh(\omega_n H)\cos[\omega_n(X-i(b-Y))]. \tag{43}$$

Numerical evaluation of Eqs. (40)–(42) shows that the EM field of the quasi-TEM mode is largely concentrated in the vicinity of the strip. It should be noted that since the quasi-TEM mode is not the pure EM mode, the electric and magnetic field amplitudes are not equal. Moreover, the transverse profiles of the electric and magnetic fields are different, and consequently, in the general case $|\vec{E}|$ and $|\vec{H}|$ could not correspond to the same point x,y of the waveguide cross section. Nevertheless, using the previous assumption of the low-frequency limit, we can use $|\vec{H}|\cong|\vec{E}|\cong A$, where the amplitude A of the EM wave was introduced in Sec. II.

The power flowing through the waveguide is defined by

$$P=\frac{c}{4\pi}\int_{S_\perp}[\vec{E}\times\vec{H}]\cdot\hat{z}\,dS_\perp. \tag{44}$$

For the quasi-TEM mode of the stripline waveguide, this power, as follows from Eqs. (40)–(42), is equal to

$$P=\frac{2\pi a}{\sqrt{\varepsilon_{\mathrm{eff}}}}\sum_{n=1,3,\ldots}\frac{\rho_n^2}{\omega_n T_n}\sinh(\omega_n(b-H))\sinh(\omega_n H), \tag{45}$$

and the norm of the wave at the input of the waveguide results in

$$N_0=\frac{4P_{\mathrm{in}}}{|\vec{E}_0||\vec{H}_0|}, \tag{46}$$

where P_{in} is the input power of the EM wave, and the subscript 0 denotes initial values.

The tapering of the waveguide parameters, as a method for efficiency enhancement, is, in particular, limited by reflections. The axial nonuniformity of the tapered stripline results in backward EM wave reflections along the waveguide which may lead to spurious oscillations due to absolute instability caused by this internal feedback. The expression for reflection coefficient Γ of the stripline waveguide, back to the input, is derived in Ref. [33]. Using normalized variables introduced in Sec. II, it can be rewritten as

$$\Gamma=-\frac{1}{2}\int_0^{\zeta_{\max}}e^{-2i(h/F)\zeta}\frac{1}{h}\frac{dh}{d\zeta}\,d\zeta, \tag{47}$$

where $\zeta_{\max}$ is the normalized length of the waveguide. Hence the assumption of a slowly varying axial wave number k_z in the tapered stripline requires that $|\Gamma|\ll 1$. This limits the general solution for the efficiency η given by Eqs. (26) and (9).

Another limitation of the analytical solution of Eq. (26) stems from the following considerations. The EM field of the stripline is largely concentrated in the vicinity of the strip. Hence, in order to design a high-efficiency device of a reasonable length L, the electron beam must be injected as closely as possible to the strip surface. On the other hand, the high efficiency of the anomalous Doppler interaction is obtained when the external magnetic field, and consequently the cyclotron frequency Ω, are small. Hence, the Larmor radius of electron rotation r_L, which is inversely proportional to Ω, may result in a large value even if the induced transverse velocity $v_\perp$ is small. In order to prevent the electron bombardment of the strip and the dielectric material, one needs to limit the device length and, correspondingly, the efficiency. These two effects contradict one another, and the contradiction results in decreasing of the AD-CRM efficiency.

IV. NUMERICAL EXAMPLE

The above analytical expressions enable one to design practical schemes of the anomalous Doppler CRM amplifier in tapered stripline structures. Figures 5–8 show results of numerical simulations of the device with the initial parameters summarized in Table I. Figure 5 shows the effective permittivity $\varepsilon_{\mathrm{eff}}$ of the tapered stripline waveguide as a function of the strip width W. The effective permittivity varies from ~30 to ~43. This corresponds to change of the normalized wavenumber h from ~5.5 to ~6.6. It should be noted that the assumption of the quasi-TEM mode limits the width of the strip W, hence it could not exceed ~5 mm for a 10-GHz frequency (the corresponding wavelength $\lambda=30$ mm).

Figures 6–8 show the output characteristics of the device in their dependence of the axial coordinate z. In these figures, the solid lines correspond to possible change of characteris-

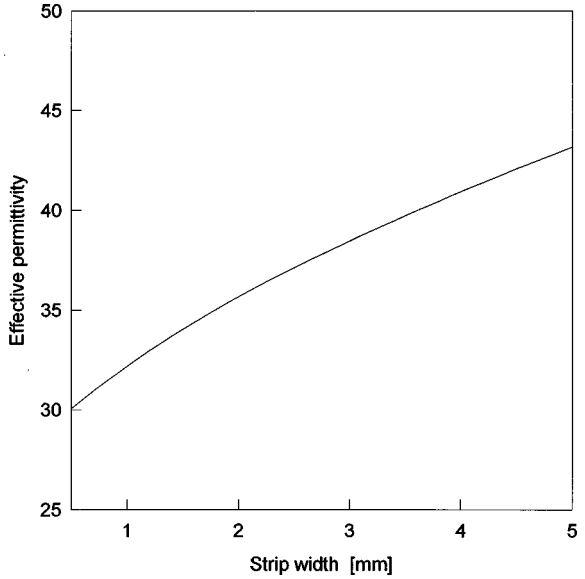

FIG. 5. The dependence of the stripline waveguide effective permittivity ε_{eff} on the strip width W. The waveguide parameters are listed in Table I.

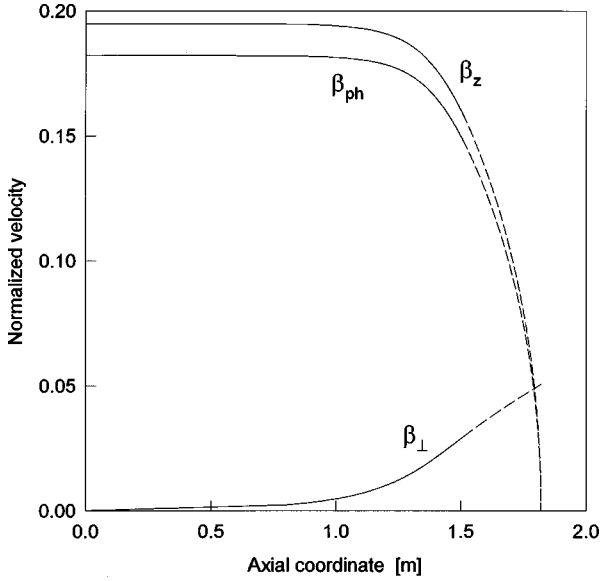

FIG. 7. The dependence of the normalized electron axial and transverse velocities β_z and $\beta_\perp$, respectively, and the EM wave phase velocity β_{ph}, on the axial coordinate z (for initial parameters as in Fig. 6).

tics taking into account the above limitations. The dashed lines show the asymptotic behavior of characteristics which cannot be realized practically in the device under consideration. Figure 6 shows the calculated values of the efficiency η and the tapered optimal normalized wave number h_{opt}. The corresponding dependencies of the normalized electron velocities β_z and $\beta_\perp$, and the EM wave phase velocity β_{ph}, are shown in Fig. 7. According to the nature of the anomalous Doppler effect, the axial electron velocity β_z is larger than the EM wave phase velocity β_{ph}. These two velocities are decreased along the z coordinate and approach zero at $z_{\max} \cong 1.8$ m. This corresponds to the complete axial deceleration of the electron. The axial evolution of the Larmor radius r_L and the number of electron gyro-orbits are shown in Fig. 8. As follows from this figure, the electron motion is characterized by a large number of gyro-orbits. Hence the highly efficient anomalous Doppler interaction in the tapered waveguide differs from those in axially uniform structures, for which a small number of electron orbits is typical.

The distance between the electron beam and the strip at the waveguide entrance is 2 mm. Hence, as follows from Fig. 8, the maximal length of the device L is limited by $\sim$1.5 m. The corresponding normalized wave number and efficiency are equal to $\sim$6.5 and $\sim$30%, respectively. The calculated reflection coefficient is small ($|\Gamma| \leqslant 0.02$). Consequently, the

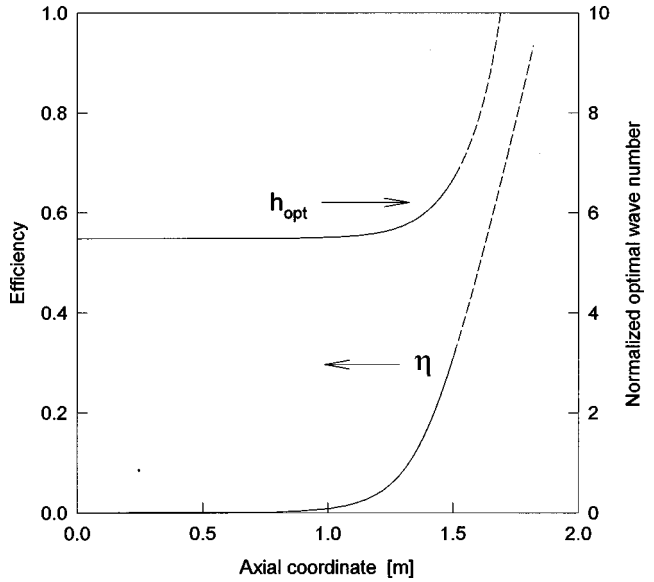

FIG. 6. The maximal efficiency η and the optimal wave number h_{opt} dependence on the anomalous Doppler CRM amplifier length L, for initial parameters listed in Table I.

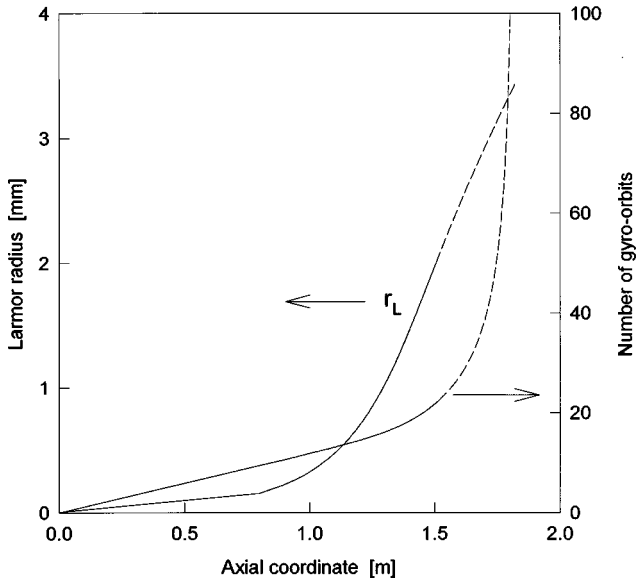

FIG. 8. The dependence of the electron Larmor radius r_L and the number of electron gyro-orbits on the axial coordinate z (for initial parameters as in Fig. 6).

TABLE I. Example of anomalous Doppler CRM amplifier parameters.

Stripline waveguide			
Dielectric substrate width	H	1	mm
Initial strip width	W_i	0.5	mm
Final strip width	W_0	5	mm
Relative dielectric permittivity	ε_r	50	
Outer tube			
Width	$2a$	70	mm
Height	b	10	mm
Length	L	1.5	m
EM wave			
Frequency	f	10	GHz
Input power	P_{in}	5	W
Electron beam			
Accelerating voltage	V_b	10	kV
Initial current	I_b	0.5	A
Position inside the waveguide	X	0	mm
	Y	3	mm
Axial magnetic field	B_0	252	G
Normalized parameters			
Initial norm of the wave (normalized)	$N_0(\omega^2/c^3)$	6.5×10^{-4}	
Initial amplitude	F_0	6.9×10^{-6}	
Initial current parameter	I	6.8×10^{5}	
	$h_0\beta_{z0}$	1.07	

proposed design of the anomalous Doppler CRM amplifier with a tapered stripline seems to be a promising scheme for further experimental realization.

V. CONCLUSION

The analytical model of an anomalous Doppler CRM amplifier with tapered waveguide parameters is derived for an EM wave of a moderate amplitude and an axially injected nonrelativistic electron beam. The linear electron beam has a better quality, and its usage simplifies the design of the anomalous Doppler CRM amplifier as compared to conventional CRM devices employing the normal Doppler effect. The tapering of the EM wave number k_z provides the conservation of the anomalous Doppler synchronism condition along the interaction region. It is shown that operation of such a device results in the high efficiency, which may asymptotically reach 100%. The electron motion is characterized by a large number of gyro-orbits.

A practical model of an anomalous Doppler amplifier using a stripline with a tapered width is proposed for a further experimental verification. The stripline waveguide has the advantage of a wide tunability. Numerical calculations show that taking into account the limitation of the amplifier's length (as explained in Sec. IV), the efficiency of this device can be about 30% for a 10-kV, 0.5-A electron beam, and a 5-W input EM power. This corresponds to a ~25-dB power gain. Hence the presented analysis forms theoretical basis for a design of the compact, low-cost, high-efficiency CRM device.

The model of an anomalous Doppler CRM with tapered parameters can be implemented to other schemes as well. In particular, other waveguides with variable dielectric loading, and tapered periodic waveguides could be considered.

ACKNOWLEDGMENT

This work was supported by the U.S.-Israel Bi-National Science Foundation (BSF) under Research Grant No. 95-00438.

[1] A. V. Gaponov, M. I. Petelin, and V. K. Yulpatov, Izv. Vyssh. Uchebn. Zaved. Radiofiz. **10**, 1414 (1967) [Radiophys. Quantum Electron. **10**, 794 (1967)].

[2] J. L. Hirshfield and V. L. Granatstein, IEEE Trans. Microwave Theory Tech. **MTT-25**, 522 (1977).

[3] R. S. Symons and H. R. Jory, Adv. Electron. Electron Phys. **55**, 1 (1981).

[4] K. E. Kreischer and R. J. Temkin, in *Infrared and Millimeter Waves*, edited by K. J. Button (Academic, New York, 1983), Vol. 7, p. 377.

[5] V. L. Bratman, N. S. Ginzburg, G. S. Nusinovich, M. I. Petelin, and P. S. Strelkov, Int. J. Electron. **51**, 541 (1981).

[6] V. L. Ginzburg and I. M. Frank, Dokl. Akad. Nauk SSSR **56**, 583 (1947).

[7] M. I. Petelin, Izv. Vyssh. Uchebn. Zaved. Radiofiz. **17**, 902 (1974) [Radiophys. Quantum Electron. **17**, 686 (1974)].

[8] V. L. Bratman and A. E. Tokarev, Izv. Vyssh. Uchebn. Zaved. Radiophys. **17**, 1224 (1974) [Radiophys. Quantum Electron. **17**, 1219 (1974)].

[9] J. R. Pierce, *Traveling-Wave Tubes* (Van Nostrand, New York, 1950), Chap. 13.
[10] N. S. Ginzburg, Izv. Vyssh. Uchebn. Zaved. Radiofiz. **22**, 470 (1979) [Radiophys. Quantum Electron. **22**, 323 (1979)].
[11] S. Yu. Galuzo *et al.*, Zh. Tekh. Fiz. **52**, 1681 (1982) [Sov. Phys. Tech. Phys. **27**, 1030 (1982)].
[12] A. N. Didenko *et al.*, Pis'ma Zh. Tekh. Fiz. **9**, 1331 (1983) [Sov. Tech. Phys. Lett. **9**, 572 (1983)].
[13] K. Ogura *et al.*, Phys. Rev. E **53**, 2726 (1996).
[14] T. H. Kho and A. T. Lin, Phys. Rev. A **38**, 2883 (1988).
[15] E. Jerby, Phys. Rev. E **49**, 4487 (1994).
[16] M. Korol and E. Jerby, Nucl. Instrum. Methods Phys. Res. A **375**, 222 (1996).
[17] G. F. Filimonov, Radiotekh. Elektron. **3**, 85 (1958) [Radio Eng. Electron. **3**, 124 (1958)].
[18] E. D. Belyavskiy, Radiotekh. Elektron. **16**, 208 (1971) [Radio Eng. Electron. Phys. **16**, 186 (1971)].
[19] N. M. Kroll, P. L. Morton, and M. N. Rosenbluth, in *Physics of Quantum Electronics*, edited by S. F. Jacobs *et al.* (Addison-Wesley, Reading, MA, 1980), Vol. 7, p. 89.
[20] P. Sprangle, C.-M. Tang, and W. M. Manheimer, Phys. Rev. A **21**, 302 (1980).
[21] N. S. Ginzburg, Izv. Vyssh. Uchebn. Zaved. Radiofiz. **30**, 1181 (1987) [Radiophys. Quantum Electron. **30**, 865 (1987)].
[22] G. S. Nusinovich, Phys. Fluids B **4**, 1989 (1992).
[23] M. Einat, E. Jerby, and A. Shahadi, Nucl. Instrum. Methods Phys. Res. A **375**, 21 (1996).
[24] M. Einat and E. Jerby, Phys. Rev. E **56**, 5996 (1997).
[25] G. S. Nusinovich and H. Li, Int. J. Electron. **72**, 895 (1992).
[26] A. W. Fliflet, Int. J. Electron. **61**, 1049 (1986).
[27] V. Ya. Davydovskii, Zh. Eksp. Teor. Fiz. **43**, 886 (1962) [Sov. Phys. JETP **16**, 629 (1963)].
[28] A. A. Kolomenskii and A. N. Lebedev, Zh. Eksp. Teor. Fiz. **44**, 261 (1963) [Sov. Phys. JETP **17**, 179 (1963)].
[29] C. S. Roberts and S. J. Buchsbaum, Phys. Rev. **135**, A381 (1964).
[30] A. V. Gaponov, Izv. Vyssh. Uchebn. Zaved. Radiofiz. **4**, 547 (1961).
[31] V. L. Bratman, N. S. Ginzburg, and A. V. Savilov, in *High-Frequency Relativistic Electronics*, edited by A. V. Gaponov-Grekhov (Institute of Applied Physics, Nizhniy Novgorod, Russia, 1992), Vol. 7, p. 22.
[32] I. S. Gradshteyn and I. M. Ryzhik, *Tables of Integrals, Series, and Products* (Academic, New York, 1980), p. 108.
[33] R. E. Collin, *Foundations for Microwave Engineering* (McGraw-Hill, New York, 1992), Chap. 3.12, and references therein, and Chap. 5.16.
[34] A. Farrar and A. T. Adams, IEEE Trans. Microwave Theory Tech. **MTT-24**, 456 (1976).
[35] J. F. Lee, D.-K. Sun, and Z. J. Cendes, IEEE Trans. Microwave Theory Tech. **MTT-39**, 1262 (1991).
[36] S.-Y. Lin and C. C. Lee, IEEE Trans. Microwave Theory Tech. **MTT-44**, 1977 (1996), and references therein.
[37] C. E. Smith and R. S. Chang, IEEE Trans. Microwave Theory Tech. **MTT-28**, 90 (1980).